A partial structure investigation on the traditional bulk metallic glass $Pd_{40}Ni_{40}P_{20}$

Shinya Hosokawa,[1,2,*] Jean-François Bérar,[3] Nathalie Boudet,[3] Wolf-Christian Pilgrim,[2] László Pusztai,[4,5] Satoshi Hiroi,[6] Kenji Maruyama,[7] Shinji Kohara,[6] Hidemi Kato,[8] Henry E. Fischer,[9] and Anita Zeidler[10]

[1]*Department of Physics, Kumamoto University, Kumamoto 860-8555, Japan*
[2]*Faculty of Chemistry, Physical Chemistry, Philipps University of Marburg, 35032 Marburg, Germany*
[3]*Institut Néel, Centre National de la Recherche Scientifique (CNRS)/University of Grenoble Alpes, 38042 Grenoble Cedex 9, France*
[4]*Wigner Research Centre for Physics, Hungarian Academy of Sciences, H-1525 Budapest, Hungary*
[5]*International Research Organization for Advanced Science and Technology, Kumamoto University, Kumamoto 860-8555, Japan*
[6]*National Institute for Materials Science, Hyogo 679-5148, Japan*
[7]*Department of Chemistry, Faculty of Science, Niigata University, Niigata 950-2181, Japan*
[8]*Institute for Materials Research, Tohoku University, Sendai 980-8577, Japan*
[9]*Institut Laue-Langevin, 38042 Grenoble Cedex 9, France*
[10]*Department of Physics, University of Bath, Bath BA2 7AY, UK*

(Dated: August 6, 2019)

Local structures of $Pd_{40}Ni_{40}P_{20}$ bulk metallic glass (BMG) were investigated by combining anomalous x-ray scattering close to the Pd and Ni K absorption edges, x-ray diffraction, neutron diffraction, and reverse Monte Carlo modeling, from which partial structure factors $S_{ij}(Q)$ and partial pair distribution functions $g_{ij}(r)$ as well as three-dimensional atomic configurations were carefully obtained around the constituent elements. A disagreement is found in the local structures with an *ab initio* molecular dynamics simulation by Guan et al., i.e., the existence of the P-P nearest neighboring configurations is clarified in the present experimental result. From the Voronoi tessellation analysis, a preference of the pure icosahedral configurations is observed around the Ni atoms, whereas the local configurations around the Pd and P atoms are rather distorted icosahedra. A persistent homology analysis was carried out to identify meaningful shape characteristics of the intermediate-range atomic configuration of large rings.

I. INTRODUCTION

$Pd_{40}Ni_{40}P_{20}$ is the historical metal-metalloid metallic glass that was discovered more than three decades ago[1,2] as the first bulk metallic glass (BMG). This glass shows an excellent glass-forming ability (GFA) with a critical cooling rate (CCR) of about 1 K/s,[2–4] which can be formed into a massive bulk glass with a diameter of about 10 mm by simple melt-quenching.[2,3] Although several thermodynamic, mechanical, structural, and electronic properties were investigated in detail for this BMG, no systematic views were obtained so far to understand why this glass has such an excellent GFA.

As regards the atomic structures, an anomalous x-ray scattering (AXS) experiment was performed by Park et al.[5] at incident x-ray energies close to the Ni K absorption edge. They obtained the differential structure factor close to the Ni K edge, $\Delta_{\rm Ni}S(Q)$, and discussed the local structure around the Ni atoms. Using the advantage of the AXS technique for the partial structures, they concluded that the existing model of trigonal prismatic packing[6] would be suitable for the local atomic arrangement around the Ni atoms.

Haruyama et al.[7] investigated again partial structures around the Ni atoms in the $Pd_{40}Ni_{40}P_{20}$ glass by Ni K AXS experiments. They analyzed differential radial distribution function around the Ni atoms, $\Delta_{\rm Ni}g(r)$, Fourier-transform of $\Delta_{\rm Ni}S(Q)$, and decomposed its first peak into three Ni-related contributions. As a result, they reported unusual remarkable changes in the coordination numbers of the Ni-Ni and Ni-Pd pairs by annealing the glass sample just above the glass transition temperature, indicating a microscopic phase separation tendency, changing to a *bct* Ni_3P-like structure. Due to the limited Q range of the $\Delta_{\rm Ni}S(Q)$, however, the Fourier-transformed peaks in real space were broadened in both of the above AXS experiments, which prevented a detailed analysis even on the first neighboring atomic configurations as mentioned in a paper on AXS.[8]

Another AXS study was carried out by Egami et al.[9] close to the Pd K absorption edge to clarify the local atomic arrangement around the Pd atoms. From the obtained $\Delta_{\rm Pd}S(Q)$, they concluded that the structure of $Pd_{40}Ni_{40}P_{20}$ glass can be described basically by a dense random packed structure with weak chemical short-range order. Based on this result, they suggested that the exceptional stability of the $Pd_{40}Ni_{40}P_{20}$ glass originates mainly from the instability of the competing crystalline phases rather than the atomic ordering in the glass, in contrast to the previous AXS study.

Hosokawa et al. also carried out AXS measurements on the $Pd_{40}Ni_{40}P_{20}$ glass close to the Pd and Ni K edges[10–13] for the comparison to the most excellent BMG, $Pd_{42.5}Ni_{7.5}Cu_{30}P_{20}$, having at present the lowest CCR of 0.067 K/s.[14] Detailed analyses of the $\Delta_i S(Q)$ functions revealed that a strong correlation between the Pd-P atoms is found in the $Pd_{42.5}Ni_{7.5}Cu_{30}P_{20}$ glass, while such a chemical correlation seems to be weak in the $Pd_{40}Ni_{40}P_{20}$ glass.

In order to clarify the role of electronic structures in the $Pd_{40}Ni_{40}P_{20}$ glass, spectroscopic measurements were performed such as incident photon energy dependence of photoemission spectroscopy, soft x-ray absorption and emission spectroscopies, and inverse-photoemission spectroscopy, and the partial density of states (DOS) of Pd 4*d* and Ni 3*d* electrons were estimated.[15–17] It was found that the DOS at the Fermi energy is mainly made of Pd 4*d* and Ni 3*d* electrons, and very small as expected from the conductivity data,[18] which seems to be consistent with the Nagel-Tauc prediction.[19] Core-level photoemission spectra were measured on Pd 3*d*, Ni 3*p*, and P 2*p* levels to investigate the chemical nature of the constituent elements, and it was found that the P 2*p* core level clearly separates into two states, indicating that the P atoms have two different chemical sites, although one site with smaller binding energy dominates.[13]

Ab initio molecular dynamics (MD) simulations were performed on $Pd_{40}Ni_{40}P_{20}$ BMG by Kumar et al.[20] and Guan et al.[21] The results were analyzed in detail using the Voronoi tessellation method[22] with an ingenious cutoff length definition around the P atoms including the electronic charge density. From these analyses, they reported a hybrid atomic packing scheme comprised of a covalent-bond-mediated stereochemical structure around the P atoms and a densely packed icosahedron around the metal atoms in this BMG. The structural features obtained from this *ab initio* MD simulation are in good agreement with slight modifications with the existing cluster models based on the structures of the approximant crystal of tricapped trigonal prism[6] around the P atoms, and icosahedral clusters[23] around the Ni atoms. At a glance, these seem to be reasonable to explain the excellent GFA of the $Pd_{40}Ni_{40}P_{20}$ BMG compared to $Pd_xNi_{80-x}P_{20}$ with different x values.

AXS is a novel method[24] that can provide partial structural information on both the short- and intermediate-range order (SRO and IRO) around each constituent element in multicomponent non-crystalline materials. However, the P-related partials are difficult to obtain since the absorption edge energy of the P element is too low to carry out AXS. On the other hand, P has a relatively large neutron scattering cross-section, helping to clarify the atomic positions of the P atoms in the glass. Thus, neutron diffraction (ND) experiments were also carried out.

In this paper, we report the local- and intermediate-range structures of $Pd_{40}Ni_{40}P_{20}$ BMG investigated by combining AXS, x-ray diffraction (XRD), ND experiments, and reverse Monte Carlo (RMC) modeling.[25] The preliminary results were already reported elsewhere in a review article.[26] From a Voronoi tessellation analysis, the preference of icosahedral configurations is confirmed around the Ni atoms rather than Pd. A persistent homology analysis was carried out to identify meaningful shape characteristics of the atomic configurations. The structural origin of the excellent GFA of this BMG is discussed using a plausible model from the experimental points of view on the partial structures.

In this article, the experimental procedure and the data analysis are given in Secs. II and III, respectively. Results of the experiments and RMC modeling are presented in Sec. IV. In Sec. V, we discuss the partial structures of the $Pd_{40}Ni_{40}P_{20}$ BMG with several structural parameters and three-dimensional (3D) atomic configurations using a Voronoi tessellation and a persistent homology analysis, and by comparing with the existing *ab initio* MD simulation. A conclusion is given in Sec. VI.

II. EXPERIMENTAL PROCEDURE

The $Pd_{40}Ni_{40}P_{20}$ rod sample with a diameter of 3 mm was prepared as follows. Prior to making the master ingot, a Pd-P pre-alloy was made using Pd and P polycrystals with purities of 99.95% and 99.9999%, respectively. Then, a master ingot was manufactured by arc-melting the mixture of pure Pd, Ni, and the pre-alloyed Pd-P in an Ar atmosphere. The purity of Ni was 99.9%. In order to eliminate heterogeneous nucleation due to oxide contamination, a B_2O_3 flux treatment[3,4] was repeatedly carried out in a highly purified Ar atmosphere. The melt was kept at about 1000°C for at least six days, and then, quenched by tilt casting into a Cu mold. The concentrations of the measured sample was examined by electron-probe micro-analysis, and the results were almost the nominal values within the experimental error of 0.2 wt.%.

The AXS technique utilizes an anomalous variation of the atomic form factor of a specific constituent element near an x-ray absorption edge of the element. The complex atomic form factor of an element is given as

$$f(Q,E) = f_0(Q) + f'(E) + if"(E), \tag{1}$$

where f_0 is the usual energy-independent term, and f' and $f"$ represent the real and imaginary parts of the anomalous term, respectively. When the incident x-ray energy E approaches an absorption edge of a constituent element, its f' has a large negative minimum and $f"$ shows an abrupt jump.

One can utilize the contrast between two scattering spectra near an absorption edge of the kth element $\Delta_k I$, where one is typically measured at some 10 eV and one at some 100 eV below the edge ($E^k_{\rm near}$ and $E^k_{\rm far}$, respectively). This differential intensity is expressed as

$$\begin{aligned}\alpha_k \Delta_k I(Q, E^k_{\rm far}, E^k_{\rm near}) &= \Delta_k[\langle f^2\rangle - \langle f\rangle^2] \\ &\quad + \Delta_k[\langle f\rangle^2]\Delta_k S(Q),\end{aligned} \tag{2}$$

where α_k is a normalization constant and $\Delta_k[\,]$ indicates the difference of values in the bracket at energies of $E^k_{\rm near}$ and $E^k_{\rm far}$ close to the absorption edge of the kth element.

The $\Delta_k S(Q)$ functions are given as a linear combination of partial structure factors $S_{ij}(Q)$,

$$\Delta_k S(Q) = \sum_{i=1}^{N}\sum_{j=1}^{N} W^k_{ij}(Q, E^k_{\rm far}, E^k_{\rm near}) S_{ij}(Q). \tag{3}$$

TABLE I. The f' and f'' values of Pd, Ni, and P in electron units at energies measured.[29] After Ref. 26.

Element	E (eV)	$f'_{\rm Pd}$	$f''_{\rm Pd}$	$f'_{\rm Ni}$	$f''_{\rm Ni}$	$f'_{\rm P}$	$f''_{\rm P}$
Pd	24320	**-5.952**	0.552	0.237	0.610	0.044	0.048
	24150	**-4.228**	0.559	0.239	0.618	0.045	0.049
Ni	8313	-0.073	3.723	**-5.706**	0.480	0.274	0.408
	8133	-0.062	3.864	**-3.403**	0.500	0.280	0.425

TABLE II. The weighting factors W^k_{ij} at $Q = 30$ nm^{-1}. After Ref. 26.

i-j	Pd-Pd	Pd-Ni	Pd-P	Ni-Ni	Ni-P	P-P
$S_{\rm X}(Q)$	0.296	0.404	0.092	0.138	0.063	0.007
$\Delta_{\rm Pd}S(Q)$	**0.537**	0.377	0.086	0.000	0.000	0.000
$\Delta_{\rm Ni}S(Q)$	0.007	**0.616**	0.002	**0.288**	**0.087**	0.000
$S_{\rm N}(Q)$	0.099	0.345	0.086	**0.301**	**0.150**	**0.019**

Here, the weighting factors $W^k_{ij}(Q, E^k_{\rm far}, E^k_{\rm near})$ are given by

$$W^k_{ij}(Q, E^k_{\rm far}, E^k_{\rm near}) = x_i x_j \frac{\Delta_k[f_i f_j]}{\Delta_k[\langle f\rangle^2]} \qquad (4)$$

where x_i is the atomic concentration of element i.

The AXS experiments were conducted using a standard $\omega - 2\theta$ diffractometer installed at the beam line BM02 of the European Synchrotron Radiation Facility (ESRF) in Grenoble, France. In order to obtain differential structure factors, $\Delta_i S(Q)$, close to the Pd and Ni K edges, two scattering experiments were performed at energies 30 and 200 eV below the Pd K edge (24.350 keV), and 20 and 200 eV below the Ni K edge (8.333 keV). The details of the experimental setup, in particular, the detecting system using a bent graphite analyzer crystal and a long detector arm, is given elsewhere.[26] As an x-ray total structure, $S_{\rm X}(Q)$, the XRD data measured at the incident energy of 24.150 keV was used.

The ND experiment was performed to obtain the neutron total structure factor, $S_{\rm N}(Q)$, using the D4c instrument[27] at the Institut Laue-Langevin (ILL) in Grenoble, France, with an incident neutron wavelength of 0.04964(1) nm. The diffraction pattern of the $Pd_{40}Ni_{40}P_{20}$ rod of 3 mm diameter was taken with the sample held under vacuum. It was corrected for background scattering, attenuation, multiple scattering, and inelastic scattering to yield $S_{\rm N}(Q)$ and the usual self-consistency check was performed.[28]

III. DATA ANALYSIS

For the AXS data analysis, Sasaki's theoretical values[29] were used for the anomalous term, and are given in Table I, which was already shown in Ref. 26. Large contrasts are seen in the f' values near the absorption edges of the corresponding elements as shown in bold. The W^k_{ij} values were calculated with these f' and f'' values together with the theoretical $f_0(Q)$ values.[30] Following the analysis procedure given in Ref. 31, the $\Delta_k S(Q)$ functions were calculated using Eqs. (1)–(4) from each pair of the scattering data.

The W^k_{ij} values at $Q = 30$ nm^{-1} near the first peak position in $S_{\rm X}(Q)$ are tabulated in Table II together with those in $S_{\rm X}(Q)$ and $S_{\rm N}(Q)$, which was already shown in Ref. 26. These values slightly change with Q in the x-ray data, while they are constant in $S_{\rm N}(Q)$. The edge-related $S_{ij}(Q)$ functions are largely enhanced in $\Delta_k S(Q)$ and the other partials are highly suppressed. Also, the P-related $S_{ij}(Q)$ are enhanced in $S_{\rm N}(Q)$. The bold numbers indicate the enhanced weighting factors compared with those in $S_{\rm X}(Q)$.

RMC modeling[25] is a useful tool to construct 3D structural models of disordered materials using experimental diffraction data. In the RMC modeling, the atoms of an initial configuration are moved so as to minimize the deviation from experimental structural data, e.g., in this study, two $\Delta_k S(Q)$, $S_{\rm X}(Q)$, $S_{\rm N}(Q)$, and the pair correlation function obtained from ND, $g_{\rm N}(r)$, using a standard Metropolis Monte Carlo algorithm.[32]

The starting configuration of a system containing 10,000 atoms with the measured number density were generated using hard-sphere Monte Carlo simulation (random configuration). To avoid unphysical atomic configurations, only the constraint of shortest atomic distances was applied, i.e., 0.20 nm between the metallic elements of Pd and Ni, and 0.18 nm for the P-related partials. The calculation cubic box length was chosen to be 5.0807 nm, corresponding to the number density of 76.25 nm^{-3} obtained by our density measurement of the present sample. The RMC modeling was performed using the RMC++ program package coded by Gereben et al.[33]

As regards the statistics of the present RMC results, the Q resolution of D4c neutron spectrometer implies a neutron coherence volume with a full-width at half-maximum (FWHM) of about 6 nm. The present RMC box size of about 5 nm is approximately equal to the FWHM of the neutron coherence volume. The XRD has a better Q-space resolution than the ND data, and therefore, the spatial correlation lengths in the glasses are in any cases equal to or smaller than the present RMC box size. Consequently, the present RMC simulation gives a satisfactory result in the atomic configurations of this metallic glass.

The topology of local atomic arrangements in non-crystalline materials is often analyzed by a Voronoi tessellation method.[34] The Voronoi cell or polyhedron of an atom contains all points in space which are closer to the center of the atom than to any other atoms. The Voronoi tessellation thus produces convex polyhedral cells, which

have planer faces and completely fill the space. The different coordination polyhedra surrounding a central atom can be characterized by the Voronoi indices (n_3,n_4,n_5,n_6, ...), where n_i denotes the number of i-edged faces of the polyhedron and $\sum_i n_i$ is the coordination number. In this study, we applied Voronoi polyhedra analysis to the atomic configurations in $Pd_{40}Ni_{40}P_{20}$ BMG generated by RMC.

Persistent homology[35] is a topological method which can extract hierarchical structures of various non-crystalline solids in the short, medium, and even further ranges. This method describes a persistent diagram (PD), a mathematical tool for capturing shapes of multi-scale data. The input to the PDs is a pair of atomic positions and input radius for each atoms, r_i. To characterize the multiscale properties, a parameter α is introduced to generate a family of atomic balls having the radius of $r_i(\alpha) = \sqrt{\alpha + r_i^2}$. With varying radii of atomic balls by changing α, rings are detected at each α. Then, there is an $\alpha = b_k$ ($\alpha = d_k$) value at which a ring k first appears (disappears) in the atomic ball model. The b_k and d_k values are called the birth and death scale of the ring k, respectively. From this construction, (b_k, d_k) encodes certain scales of each ring, i.e., b_k indicates the maximum distance between two adjacent atoms in the ring, whereas d_k represents the size of ring. The output is expressed as two-dimensional histograms of b_k and d_k. There are two types of persistent homology analysis at present. One is counting ring structures named D1 and another is counting three-dimensional cavities named D2. Only the ring structure D1 is presented in this paper. Details of the PD analysis are given in elsewhere.[35]

IV. RESULTS

Circles in Fig. 1(a) show the experimental data of $\Delta_{Pd}S(Q)$ and $\Delta_{Ni}S(Q)$ taken from AXS together with $S_X(Q)$ and $S_N(Q)$ in the whole Q range measured, and Fig. 1(b) shows in the small Q range for the clarity. Consistencies with previous results are seen in the features of $S_X(Q)$[7,9] and $\Delta_{Ni}S(Q)$.[5,7] As seen in the figure, all of the structure factors resemble each other. However, interesting features are already observed from a detailed inspection of these data. 1) The first peaks in $\Delta_{Ni}S(Q)$ and $S_N(Q)$ locate at Q values higher than those in $\Delta_{Pd}S(Q)$ and $S_X(Q)$. 2) The second and third maxima in $S_N(Q)$ are shifted towards the higher Q values with respect to the $S_X(Q)$ and $\Delta_{Pd}S(Q)$ data. 3) A slight enhancement is observed in $S_N(Q)$ at low Q values. All of these differences result from the different weighting factors of the different experimental methods shown in Table II.

Solid curves in Fig. 1 show the corresponding fits from RMC modeling. Although the experimental spectra have each characteristic features, the RMC results are in good agreement with all of the experimental data within the experimental errors.

Circles in Fig. 2 represent the experimental data of

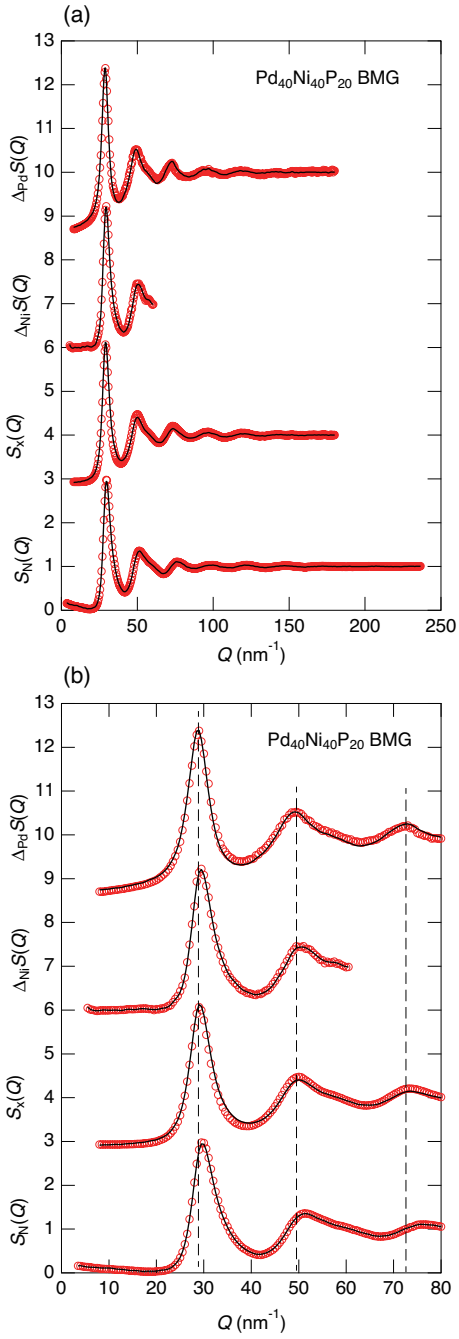

FIG. 1. (Color online.) From top to bottom, circles denote experimental data of $\Delta_{Pd}S(Q)$ and $\Delta_{Ni}S(Q)$ taken from AXS, and $S(Q)$s by XD and ND in the (a) whole Q range measured and (b) in the low Q range up to 80 nm^{-1}. Solid curves show the corresponding fits from RMC modeling. For clarity, the spectra are displaced upwards by 3.

$g_N(r)$ and the solid curve shows the corresponding fit from RMC modeling. As seen in the figure, the RMC fit excellently reproduces again the experimental data. The first peak in $g_N(r)$ has a main peak at 0.263 nm and a shoulder at the smaller r value of about 0.23 nm. The height of the shoulder is larger than in the XRD

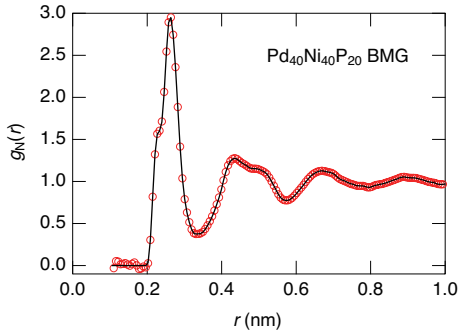

FIG. 2. (Color online.) Circles represent experimental $g_{\rm N}$ data and the solid curve shows the corresponding fit from RMC modeling.

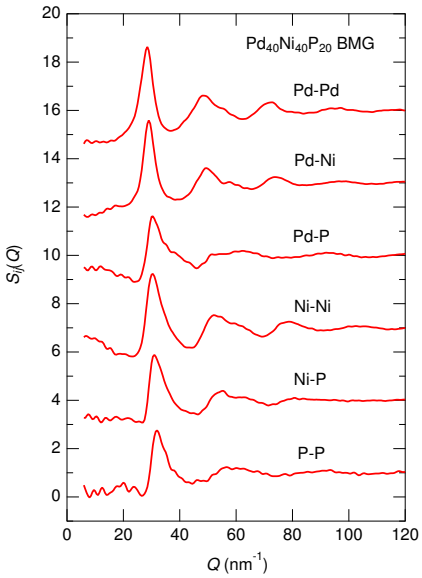

FIG. 3. (Color online.) $S_{ij}(Q)$s obtained from the RMC calculation. For clarity, the spectra are displaced upwards by 3.

measurements,[7,9,13] which is owing to the difference in the weighting factors between XRD and ND.

Figure 3 shows the partial structure factors, $S_{ij}(Q)$, obtained from the RMC modeling. The features of $S_{ij}(Q)$ highly depend on the combinations of partial elements. Firstly, the first peak positions of $S_{ij}(Q)$ are different from each other, ranging from 28.5 nm^{-1} in Pd-Pd to 31.9 nm^{-1} in P-P. Secondly, the first peak of $S_{\rm PdPd}(Q)$ has a small tail at the low Q side, indicating the existence of a weak Pd-Pd intermediate-range correlations, although the total $S_{\rm X}(Q)$ and $S_{\rm N}(Q)$ have no indications. However, the existence of a larger shoulder was observed in $S_{\rm PdPd}(Q)$ in the same Q range by the previous report of $\Delta_{\rm Pd}S(Q)$ when the Ni atoms are replaced by the Cu atoms.[10–13]

On the other hand, the Ni-related $S_{ij}(Q)$ have tails in the higher Q ranges of their first peaks. This feature suggests that the environments around the Ni atoms cannot be described by a simple dense-packed hard-sphere scheme, but the Ni atoms have plural interatomic distances with the nearest neighboring atoms regardless to the elements.

A tendency of phase separation is clearly seen in the Ni-Ni correlation as an enhancement of $S_{ij}(Q)$ in the low Q region. The relationship between a small angle intensity enhancement and a phase separation in metallic glasses was firstly studied by Chou and Turnbull[36] on the temperature dependence of Pd-Au-Si metallic glasses, which shows a separation into two melts with different concentrations. The relationship in a Pd-Ni-P alloy was investigated by Yavari et al.[37] These studies were, however, carried out in a very small Q range around 0.1 nm^{-1}, corresponding to a long r range of more than several 10 nm. In the present study, the enhancement of structure factor intensity appears at about 5 nm^{-1}, corresponding to the r range of about 1 nm. In the present study, the concentration saparations are prominent, while the density fluctuations are not so large as indicated in $S_{\rm N}(Q)$.

The $S_{\rm PdP}(Q)$ function shows a small first peak with a large shoulder in the higher Q range followed by a highly damped second peak. A phase separation tendency is also observed in this correlation. The $S_{\rm PP}(Q)$ function looks similar to $S_{\rm PdP}(Q)$. However, the enhancement in the low Q region is replaced by a broad prepeak at about 20 nm^{-1}, indicating a weak intermediate-range order between the P atoms.

The P-P correlation has the largest errors owing to the smallest weighting factor even for the ND data of 1.9% as in Table II. Nevertheless, the prepeak height is about double the noise level of ripples around the prepeak. A series of RMC calculations was carried out, where the sum of the well-saturated results showed the same features such as ripples in the resultant $S_{ij}(Q)$ functions. Thus, it is suggested that the errors in $S_{ij}(Q)$ do not originate from the RMC calculations but from the statistical errors of the experiments.

Figure 4 shows partial pair distribution functions, $g_{ij}(r)$, obtained from the RMC model. The importance of including the ND data to discuss the P-related $g_{ij}(r)$ was demonstrated by showing the weighting factors in Table 4 and comparing to the RMC results in Fig. 5 of Ref. 26. These are due to the double contributions of the Ni-P and P-P partials to $S_{\rm N}(Q)$ compared with those in the x-ray functions of XRD and AXS. In addition, unphysical sharp peaks usually appearing at the shortest interatomic distances seem to be highly suppressed by including the $g_{\rm N}(r)$ data in the RMC simulation procedure.

Since the first peak regions in $g_{ij}(r)$ are not simple peaks, the partial nearest neighbor distances r_{ij} were obtained from the average values of $g_{ij}(r)$ in the first neighboring regions, and are tabulated in Table III together with previous experimental and theoretical results. The first neighboring regions are defined in the r range up to

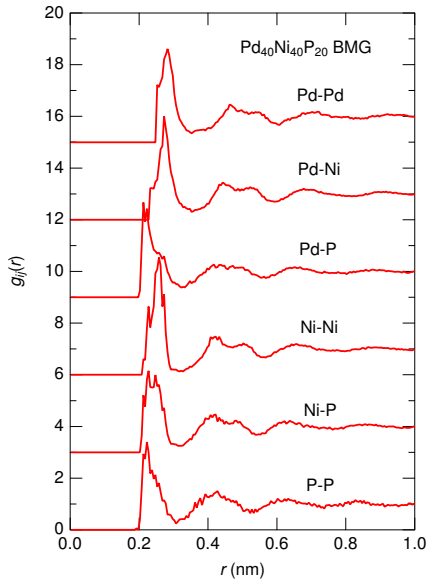

FIG. 4. (Color online.) $g_{ij}(r)$s obtained from the RMC calculation. For clarity, the spectra are displaced upwards by 3.

the first minimum in each $g_{ij}(r)$; 0.35 nm for Pd-Pd and Pd-Ni, 0.32 nm for Pd-P, Ni-Ni, and Ni-P, and 0.31 nm for P-P correlation. The values are mainly determined by the different atomic radii of the constituent elements. There are, however, characteristic features in each $g_{ij}(r)$ function, which cannot be explained by only the dense-packed hard-sphere scheme.

The $g_{\mathrm{PdPd}}(r)$ function seems to be a typical dense-packed hard-sphere structure in the sharp prominent first peak area located at 0.286(2) nm although a shoulder is observed in the lower r range. However, the second peak at 0.46(1) nm has a shoulder in the higher r range of 0.54(1) nm, which may indicate a specific cluster formation of the Pd sublattice. The $g_{\mathrm{PdNi}}(r)$ function shows a feature similar to $g_{\mathrm{PdPd}}(r)$, although r_{PdNi} is a smaller value of 0.278(2) nm. The second peak at 0.43(1) nm has a shoulder at the higher r values of 0.52(1) nm, which shows again the possibility of a cluster formation.

Egami et al.[9] calculated the $g_{\mathrm{PdPd}}(r)$ and $g_{\mathrm{PdNi}}(r)$ functions from the Pd K edge AXS experiment. The peak positions of these partials are in good agreement with the present results within the experimental errors. The spectral features also look similar to the present results except that they have a larger shoulder of the second peak in $g_{\mathrm{PdPd}}(r)$.

The first peak in the $g_{\mathrm{PdP}}(r)$ shows the most curious features among those of the $g_{ij}(r)$ functions, which has a sharp peak at about 0.22 nm with a broad shoulder centered at about 0.26 nm, and the average value is 0.245(5) nm. It should be noted that the P $2p$ core-level PES spectrum clearly separates into two states, indicating that the P atoms have two different chemical sites.[13] Such a double result in the electronic states may be consistent with the present bimodal structural data in the first neighboring peak in $g_{\mathrm{PdP}}(r)$. Concerning the second peak at 0.43(1) nm and its shoulder at 0.50(1) nm, the intensities are much lower than those of other partials.

A sharp first peak in the $g_{\mathrm{NiNi}}(r)$ is located at 0.253(2) nm followed by a prominent second peak at 0.43(1) nm with a clear shoulder at 0.51(1) nm. The $g_{\mathrm{NiP}}(r)$ function has features similar to $g_{\mathrm{NiNi}}(r)$ with a slightly lower height of the first peak. The positions of the first and second peaks and the shoulder are 0.246(3), 0.41(1), and 0.49(1) nm, respectively, slightly shorter than those of $g_{\mathrm{NiNi}}(r)$.

Haruyama et al.[7] measured AXS of $Pd_{40}Ni_{40}P_{20}$ BMG and decomposed the first peak of the Fourier transform of $\Delta_{\mathrm{Ni}}S(Q)$ into three components, Pd-Ni, Ni-Ni, and Ni-P. Although its peak shapes are broad due to the limited Q range of $\Delta_{\mathrm{Ni}}S(Q)$ up to 76 nm^{-1}, the Pd-Ni and Ni-Ni interatomic distances shown in Table III coincide well with the present results. For the Ni-P interatomic distance, a smaller r_{ij} value of 0.235(1) nm by about 0.1 nm was obtained. Since the W_{NiP} value in $\Delta_{\mathrm{Ni}}S(Q)$ is only 0.087, much smaller than W_{PdNi} and W_{NiNi} as seen in Table II, however, the present result including the ND information is more reliable.

Park et al.[5] also estimated r_{ij} from their Ni K edge AXS experiment based on a topological short range order model using a crystal-like cluster of trigonal prism capped with three half octahedra. However, they gave only the averaged values of Pd and Ni metallic elements (M) for the neighboring atoms. The r_{PdM} value of 0.268 nm is much shorter than our and Egami et al.'s results of about 0.282-4 nm, and the r_{NiM} value of 0.265 nm is mostly the present average value of 0.282 and 0.253 nm for our Pd-Ni and Ni-Ni distances, respectively. It can again be mentioned that the existence of $\Delta_{\mathrm{Pd}}S(Q)$ would be essential to correctly determine the local environment around Pd.

X-ray absorption fine structure (XAFS) results were given in Ref. 20. However, only the ranges of the first peaks are given, but coincide with the general trend of the peak positions with the elemental correlations. Exceptionally, the peak value of 0.228 nm was given the Ni-P distance in the text, which is again shorter than the present result.

An *ab initio* MD simulation by Guan et al.[21] obtained r_{ij} values which are tabulated at the bottom of Table III. The general features of element dependence in r_{ij} looks reasonable. However, all of the r_{ij} values are relatively small beyond the error bars by comparing with the results of the present experiment as well as the other experimental data.[7,9] The existence of the P-P correlations will be discussed later.

The partial coordination numbers, i.e., those of jth element around ith atom, N_{ij}, and their sum around each ith atom, $\langle N_i \rangle$, were calculated from the $g_{ij}(r)$ functions by integrating up to the minimum positions, 0.35 nm for Pd-Pd and Pd-Ni, 0.32 nm for Pd-P, Ni-Ni, and Ni-P, and 0.31 nm for P-P correlation, and the results are given in

TABLE III. The partial nearest neighbor distances r_{ij} in nm obtained from the present experiments with the RMC modeling together with previous experimental and theoretical results.

i-j	Pd-Pd	Pd-Ni	Pd-P	Ni-Ni	Ni-P	P-P	Ref.
Experiment							
AXS/XRD/ND	0.286(2)	0.278(2)	0.245(5)	0.253(2)	0.246(3)	0.240(3)	Present
AXS($\Delta_{\rm Pd}S(Q)$)	0.285(2)	0.282(2)	–	–	–	–	9
AXS($\Delta_{\rm Ni}S(Q)$)	–	0.281(1)	–	0.257(2)	0.235(1)	–	7
Theory							
Ab initio MD	0.280(2)	0.266(2)	0.241(2)	0.253(2)	0.224(2)	–	21

Table IV. The fraction of N_{ij} around the element i are given in the table below the N_{ij} values.

The total $\langle N_i \rangle$ values around the Pd, Ni, and P atoms are about 13.9, 11.9, and 10.2 atoms, respectively, which indicate mostly typical dense-packed values of 12, or a slightly different depending on the atomic radii of the elements. When the elemental portions are examined in detail, an interesting feature appears, i.e., the numbers of the Pd neighboring atoms are always larger than the nominal value of 40% by about 2%, those of the Ni neighboring atoms mostly nominal values of 40%, and those of the P neighboring atoms smaller than the nominal value of 20% by about 2%.

There are a few experimental data on the coordination numbers. The Pd K edge AXS by Egami et al.[9] gave $\langle N_{\rm Pd} \rangle = 15.3$, larger than the present result. The Ni K edge AXS by Haruyama et al.[7] provided the Ni-related partial information. The Ni atoms is slightly preferable to connect with Ni rather than Pd, contradicting the present result. Moreover, the $N_{\rm NiP}$ value (27.6%) is too large as compared to the nominal value of 20%, which is again inconsistent with the present result.

Park et al.[5] also estimated N_{ij} from their Ni K edge AXS experiment based on a topological short range order model. Their Pd-M, Ni-M, and P-M values are 11.1, 11.4, and 8.7, respectively. Compared with the present results of about 11.4, 9.8, and 8.3, the Pd-M and P-M values are consistent, while the Ni-M value is very large. They fitted a crystal-like cluster model representing a simple dense packing to $g_{\rm X}(r)$ and $\Delta_{\rm Ni}g(r)$, which may overestimate the partial coordination number around the Ni atoms.

The $\langle N_i \rangle$ values obtained by the *ab initio* MD simulation[21] of 13.6, 12.2, and 8.9 around the Pd, Ni, and P elements, respectively, are also shown in Table IV. The values around the Pd and Ni atoms are in good agreement with the present experimental results. However, the value around the P atoms is much smaller than the present experimental one.

V. DISCUSSION

The bond angle distributions are helpful to examine the IRO in this BMG. Figure 5 shows a part of the partial bond angle distributions, $\eta(\cos\theta_{ijk})$, where θ_{ijk} is the bond angle of *i*-*j*-*k* atoms. In the figure, only nine η spectra with not more than two elements are selected among totally eighteen η spectra. The $\cos\eta(\theta_{ijk})$ ($i \neq j \neq k$) result is mostly the average of $\eta(\cos\theta_{iji})$ and $\eta(\cos\theta_{kjk})$.

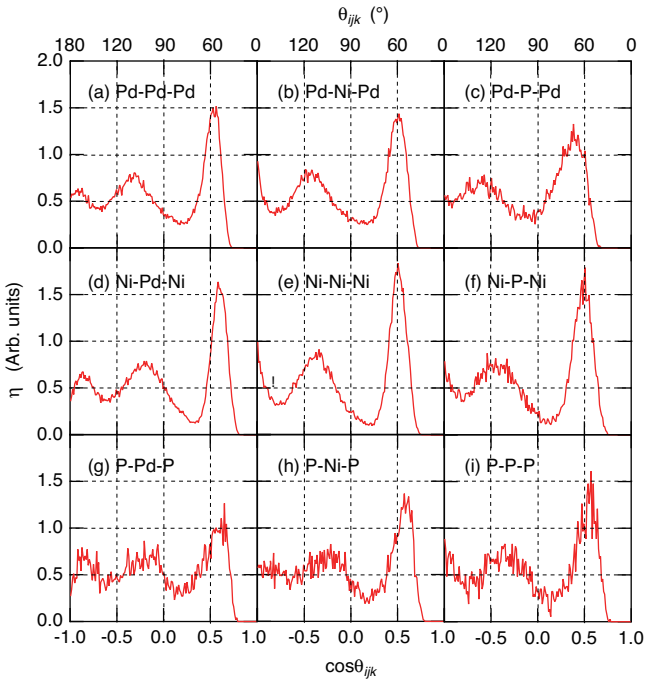

FIG. 5. (Color online.) Selected partial bond angle distributions $\eta(\cos\theta_{ijk})$. The θ_{ijk} values are given at the top of the figures.

The prominent peak is observed at about $\theta_{ijk} = 60°$, indicating that the atomic arrangements are mostly dense-packed for all the elements. The peak positions of the $\eta(\cos\theta_{iii})$ spectra are exactly 60° as shown in Fig. 5(a) Pd-Pd-Pd, (e) Ni-Ni-Ni, and (i) P-P-P. However, shifts are observed in $\eta(\cos\theta_{jij})$, suggesting the differences in the atomic radii R_i of the elements, $R_{\rm Pd} > R_{\rm Ni} > R_{\rm P}$, i.e., the peak positions in $\eta(\cos\theta_{jij})$ are less than 60° when $R_j < R_i$ as in (d) Ni-Pd-Ni, (g) P-Pd-P, and (h) P-Ni-P, and vice versa as in (b) Pd-Ni-Pd, (c) Pd-P-Pd,

TABLE IV. The total and partial average coordination numbers ($\langle N_i \rangle$ and N_{ij}, respectively) and the fractions around the elements i obtained from the present experiments with the RMC modeling together with previous experimental and theoretical results.

	$\langle N_{\rm Pd} \rangle$	$N_{\rm Pd-Pd}$	$N_{\rm Pd-Ni}$	$N_{\rm Pd-P}$	$\langle N_{\rm Ni} \rangle$	$N_{\rm Ni-Pd}$	$N_{\rm Ni-Ni}$	$N_{\rm Ni-P}$	$\langle N_{\rm P} \rangle$	$N_{\rm P-Pd}$	$N_{\rm P-Ni}$	$N_{\rm P-P}$	Ref.
Experiment													
Present	13.88(3)	5.82(2)	5.57(2)	2.49(5)	11.87(3)	4.95(2)	4.81(2)	2.11(4)	10.23(6)	4.21(5)	4.13(5)	1.90(8)	
		41.9%	40.1%	18.0%		41.7%	40.5%	17.8%		41.1%	40.4%	18.5%	
AXS($\Delta_{\rm Pd}S(Q)$)	15.3				–				–				9
AXS($\Delta_{\rm Ni}S(Q)$)	–				13.4(9)	4.7(2)	5.0(7)	3.7(5)	–				7
						35.1%	37.3%	27.6%	–				
Theory													
ab initio MD	13.6				12.2				8.9			0.0	20

and (f) Ni-P-Ni.

The second peaks in $\eta(\cos\theta_{ijk})$ are located between 100° in (d) Ni-Pd-Ni, (g) P-Pd-P, and (h) P-Ni-P, and 120° in (c) Pd-P-Pd, suggesting the differences of R_i around the Pd, Ni, and P atoms centered at the tetrahedral value of about 110°. These differences in the second peak positions can also be explained by the differences of R_i among the Pd, Ni, and P elements.

By looking at Fig. 5 in detail, only the Pd-P correlations of (c) Pd-P-Pd and (g) P-Pd-P exhibit the characteristic feature that the prominent peak at about 60° is very broad in comparison with the others. This relates to the double peak feature of the first peak in $g_{\rm PdP}(r)$ shown in Fig. 4.

Until 1970s, a widely accepted structural model for metallic glasses was that of Bernal's dense random packing of hard spheres.[38] After 1980s, however, a covalent nature in metal-metalloid metallic glasses was theoretically considered to be important in TM-B and TM-P alloys (TM: transition metals, Fe, Ni).[39,40] The P concentration dependence of TM-P alloys in the GFA was investigated by Chen,[41] and about 20 at.% P gives good GFA in any TM-P glassy alloys. On the other hand, this result indicates that a stronger covalent nature by a larger P concentration does not induce a better GFA.

Thus, it is now interesting to examine the effect of a different ternary addition,[42] which as a result produces static and dynamic heterogeneity in metallic glasses.[43,44] The existence of two chemical environments around the P atoms in the $Pd_{40}Ni_{40}P_{20}$ alloys was observed by the P 2*p* core-level photoemission spectroscopy,[13] indicating a curious double nature of the P atoms and may be related to the coexistence of metallic and covalent properties shown by the *ab initio* MD simulation by Kumar et al.[20] and Guan et al.[21]

It should be noted that the P-P interatomic correlation is observed in the present partial structural study although the fraction of the coordination number is smaller than the nominal value as shown in Table IV. To examine the existence of the P-P short bonds, another RMC fit was carried out without the P-P correlations in the first neighboring shell by setting a longer P-P cut-off length of 0.32 nm. The sum of the square of residual errors, χ^2, with no P-P short bonds was slightly larger than that with the P-P interactions by 11.9%, and in particular, the inconsistency appears in $S_{\rm N}(Q)$ by about 74% in the χ^2 value. Also, the resultant $g_{\rm PP}(r)$ has a large and unphysical peak just beyond the cut-off distance of the constraint. These experimental results suggest that P-P correlations exist within the first neighboring shell. However, a disadvantage of the RMC modeling is widely known as an energetically insensitive method, i.e., no interatomic potentials are included in the algorithm.

On the contrary, the previous *ab initio* MD simulation emphasized the lack of the P-P bonds.[20,21] They showed that their results can be described in terms of P-centered polyhedra. They also investigated the structures experimentally using high-energy XRD, and Pd and Ni *K* XAFS experiments, and wrote in this article, "the absence of a short $g_{\rm PP}(r)$ peak in the pair distribution function (PDF) suggests that direct P-P bonds are rare in this alloy."[21] This description, however, overestimates the potentials of these experimental techniques. Owing to a very small $W_{\rm PP}$ value of 0.7% for XRD as shown in Table II, however, the P-P signal in the total $g_{\rm X}(r)$ can be in a noise level of the Fourier transform from the experimental $S_{\rm X}(Q)$ data. The Pd (Ni) *K* XAFS can only observe the atomic arrangements around the central Pd(Ni) atoms. Thus, it is difficult to prove the existence of short P-P bonds by their XAFS measurements.

Thus, there is no experimental proof of P-P correlations in the first coordination shell to support either the present experiments or the recent *ab initio* MD simulation. To our knowledge, the experimental method to examine the P-P correlations is only XAFS experiment near the P *K* edge (2.149 keV) as carried out by Sheng et al.[44] Nevertheless, it is not easy to reach the conclusion because 1) the XAFS oscillation intensity by P is very small compared with those of Pd and Ni, 2) the k range of the P *K* XAFS oscillations is limited due to the experimental setup under vacuum, and 3) the decreasing k dependence of the backscattering amplitude of P is simi-

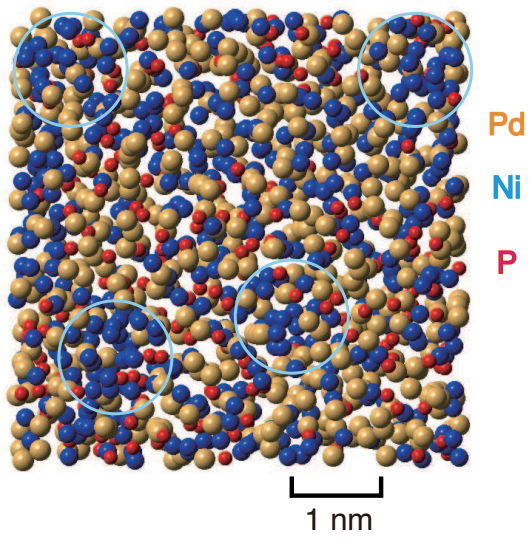

FIG. 6. (Color online.) 3D atomic representation obtained from the RMC calculation. The circles indicate the Ni-rich regions, and their diameter of 1.26 nm corresponds to a Q value of 5 nm^{-1}.

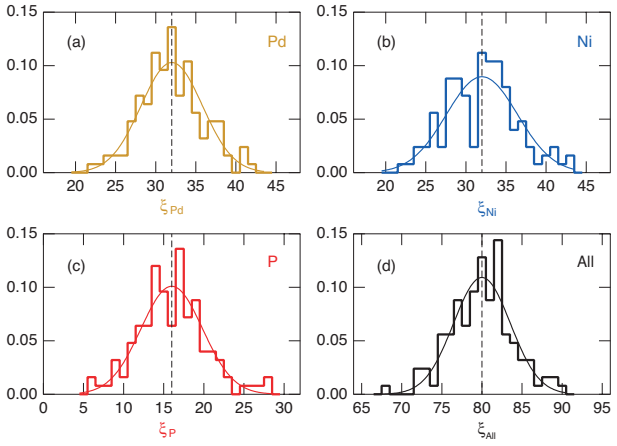

FIG. 7. (Color online.) σ_i of (a) Pd, (b) Ni, (c) P, and (d) all atoms in voxels with the size of 1.0161 nm.

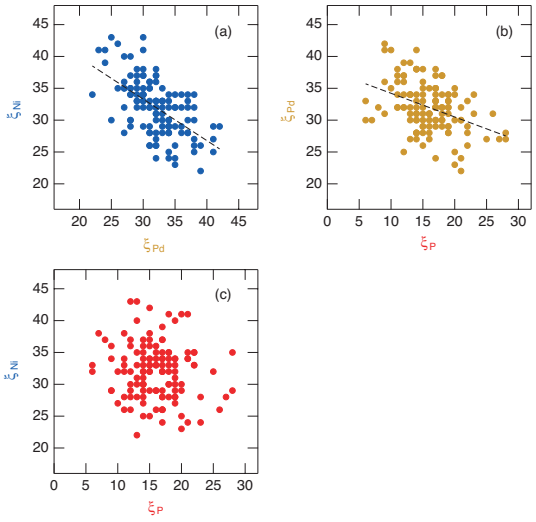

FIG. 8. (Color online.) The relation of ξ_i values between (a) Pd-Ni, (b) Pd-P, and (c) Ni-P atoms. The dashed lines in (a) and (b) indicate the data fits of linear relations.

lar to that of Pd in the low k range. Therefore, a detailed inspection of the P K XAFS experiment is essential to reach the conclusion, which is now in progress.

Figure 6 shows a 3D atomic representation obtained from the present RMC fit, where large, medium, and small balls indicate the Pd, Ni, and P elements, respectively. At a glance, the Ni atoms seem to show a slight cluster formation. The circles indicate Ni-rich regions with a diameter of 1.26 nm corresponding to a Q value of 5 nm^{-1}. The size of the separation of Ni atoms shown as the low-Q enhancement in $S_{\rm NiNi}(Q)$ is comparable to the size of the circles. Such a trend is always observed, i.e., it is not a special properties in $Pd_{40}Ni_{40}P_{20}$ alloy, but is seen in metallic glasses in general.[45–47]

To clarify the heterogeneity of the elemental concentrations quantitatively, the RMC simulation box with the length of 5.0807 nm was separated into $5 \times 5 \times 5 = 125$ voxels, and the numbers of each element were counted. Figure 7 shows the atomic number distributions ξ_i of (a) Pd, (b) Ni, (c) P, and (d) all atoms in voxels with the size of 1.0161 nm. The averages are shown by dashed lines in the figures, 32, 32, 16, and 80 atoms for Pd, Ni, P, and all atoms, respectively. To find the concentration heterogeneity, fits were carried out by using Gauss functions, and the standard deviations, σ_i, are calculated to be 5.4, 6.3, 5.4, and 5.0 atoms for Pd, Ni, P, and all atoms, respectively. As seen in these values, the positional fluctuations of Ni is larger than those of Pd.

Since the $\sigma_{\rm All}$ value is not large, a special relation is expected between the ξ_i values of the elements. Figure 8 shows the relation of ξ_i values between (a) Pd-Ni, (b) Pd-P, and (c) Ni-P atoms. The dashed lines in (a) and (b) indicate the data fits of linear relations. The Pd-Ni in (a) shows a linear relation with a slope of -0.65 ± 0.08 as shown by the dashed line. If this metallic glass is formed by dense-packed hard-spheres with the radii of 0.286 and 0.253 nm for Pd and Ni, respectively, obtained from the present r_{ij} valued in Table III, the slope should be $-(0.253/0.286)^3 = -0.69$, which is mostly in good agreement with the above experimental result of -0.65 ± 0.08.

As shown in (b), a linear relation between the Pd and P atoms is obtained with a slope of -0.37 ± 0.08. Since the prediction of dense-packed configurations gives a slope of $-(0.240/0.286)^3 = -0.59$, weak correlations, such as covalent bondings, are expected between the Pd and P atoms. In (c), ξ_i shows no relation between the Ni and P atoms, and thus, the correlations between Ni and P seem to be stronger than those between Pd and P.

TABLE V. Results of Voronoi tessellation around the Pd, Ni, and P elements beyond the fraction of 3%. The errors of the fraction are about 0.2%.

Element	$(n_3\ n_4\ n_5\ n_6\ n_7)$	Fraction (%)	$N = \sum_i n_i$
Pd	(0 2 8 4 0)	5.7	14
	(0 2 8 5 0)	4.8	15
	(0 1 10 4 0)	4.3	15
	(0 3 6 6 0)	3.2	15
	(0 1 10 3 0)	3.0	14
Ni	(0 1 10 2 0)	10.1	13
	(0 3 6 4 0)	7.5	13
	(0 2 8 4 0)	7.2	14
	(0 0 12 0 0)	**5.8**	12
	(0 1 10 3 0)	3.6	14
	(0 2 8 2 0)	3.5	12
	(0 3 6 5 0)	3.5	14
P	(0 2 8 2 0)	6.9	12
	(0 2 8 1 0)	6.0	11
	(0 3 6 4 0)	6.0	13
	(0 3 6 3 0)	4.6	12

Table V shows the results of Voronoi tessellation around the Pd, Ni, and P elements. For the dense-packed atomic configurations, the non-crystalline feature is characterized by icosahedral atomic configurations with Voronoi indices of (0 0 12 0), while crystalline configurations corresponding to the *fcc* and *hcp* structures both have Voronoi indices of (0 12 0 0).

As seen in the table, five-edged faces dominate Voronoi indices around all of constituent elements. Thus, icosahedra-like atomic configurations dominate the local structure of the $Pd_{40}Ni_{40}P_{20}$ BMG. However, the pure icosahedral (0 0 12 0) configurations can be mainly seen around the Ni atoms with a fraction of 5.8(2)% as indicated by the bold number. Moreover, the largest fraction of 10.1% around Ni is found for the index (0 1 10 2 0), which is a very slightly deformed icosahedron by adding only one atom to a perfect one. On the other hand, 0.3% (2.3%) and 2.5% (2.9%) of pure (slightly deformed) icosahedra are observed around the Pd and P atoms, respectively, and most of the local structures around them are deformed from the icosahedral atomic configurations. The preference of pure icosahedra around Ni may be related to the excellent GFA of this traditional BMG.

Figure 9 shows the persistence diagram, i.e., the birth-death map obtained from the persistent homology analysis, for the ring structure around (a) all atoms, (b) Pd, (c) Ni, and (d) P elements. As shown in (a), the birth-death points are distributed just above the diagonal slope line, showing a typical feature of random distribution of the atoms, which was examined by using a Lenard-Jones glassy system in Fig. 7 of Ref. 35.

When the partial persistence diagram is shown around (b) Pd and (c) Ni atoms, a different feature rises up in the map, i.e., a distinct contribution appears in the area of short-birth and long-death as indicated by arrows, which reveals the existence of large rings with the Pd or Ni atoms. A similar result was obtained in Zr-Cu glasses around the Zr atoms as shown in Fig. 8 of Ref. 35, where the atomic configurations were obtained by using a classical MD simulation. Since the Zr-Cu alloys can form a BMG phase, it is possible that the existence of such large rings reflects a good GFA. It should be noted that to our knowledge, the present work is the first experimental one that shows the existence of such large rings. To confirm this relation, an RMC calculation and the subsequent persistent homology analysis are essential on metallic glasses with a poor glass-forming ability such as $Pd_{40}Cu_{40}P_{20}$ alloy or simple liquid metal alloys like Na-K system, which is now in progress. Note that the persistent homology analysis is a simple and promising method to investigate an intrinsic character of intermediate-range atomic configurations in metallic glasses.

The persistence diagram around the P atoms are rather scattered as shown in Fig 9(d). Owing to a small concentration and a heterogeneous distribution of P, distinct ring structures cannot be detected by the present persistent homology analysis even though the P-P partial structures are correctly obtained by the ND experiment. A detailed *ab initio* MD simulation is necessary to catch the proper intermediate-range structural information around the P atoms.

The final goal of the present partial structural study is to find a clear relationship between the atomic structural features and the GFA of metallic glasses. Characteristic features in the intermediate-range atomic arrangements of the $Pd_{40}Ni_{40}P_{20}$ glass with the excellent GFA, such as the preference of the perfect icosahedral structures around the Ni atoms and the existence of large rings composed of the Pd and Ni atoms, may be related to the excellent GFA. At present, however, this work shows the first systematic and reliable result of the atomic structures in metallic glasses, and there are no reference work of other metallic glasses so far for the comparison with the present study. To examine this idea, a systematic work is necessary on partial structures of, e.g., $Pd_{40}Cu_{40}P_{20}$, which has similar constituent elements but exhibits a worse GFA, where a cooling rate of 100 K/s is required to form a BMG rod with 7 mm diameter,[48] and $Pd_{42.5}Ni_{7.5}Cu_{30}P_{20}$, which is mostly a mixture of the above alloys and shows a champion CCR of 0.067 K/s at present.[14] These works are now in progress.

VI. SUMMARY

AXS and ND experiments were performed on the traditional bulk metallic glass $Pd_{40}Ni_{40}P_{20}$ alloy to investigate the short- and intermediate-range partial structures around each constituent element, and the results were carefully analyzed using RMC modeling. The partial interatomic distances agree with the existing XAFS and

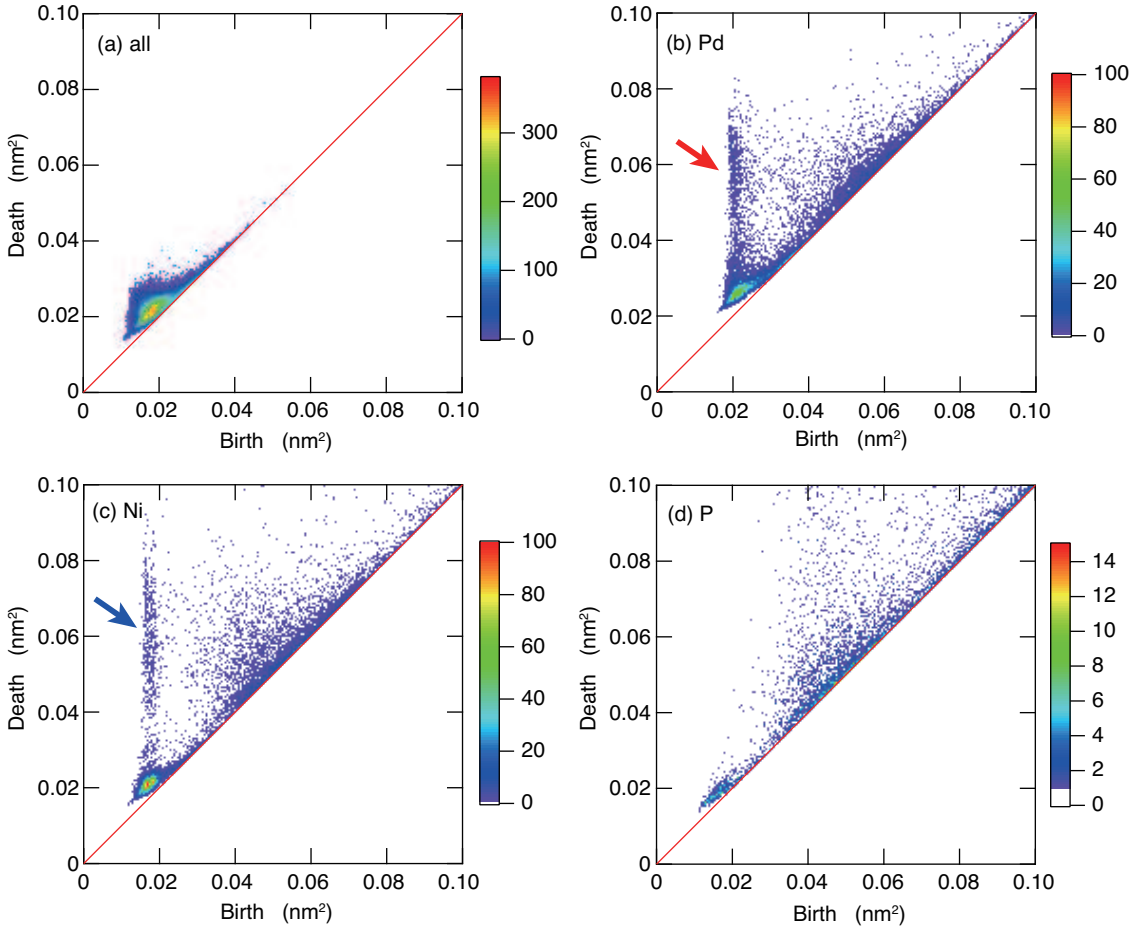

FIG. 9. (Color online.) The persistence diagram for the ring structure D1 around (a) all atoms, (b) Pd, (c) Ni, and (d) P elements.

AXS results. The partial coordination numbers obtained from the present RMC modeling are physically reasonable, despite the disagreements with the previous works. In particular, an inconsistency is found in the local structures against the *ab initio* MD simulation by Guan et al.[21], i.e., the existence of the P-P nearest neighboring configurations is clearly obtained in the present model. The result of Voronoi tessellation clarifying the short-range atomic environments shows a clear difference in that the Ni atoms prefer to form pure icosahedral atomic configurations, while local structures around the Pd and P atoms are deformed. The partial persistent homology analysis for investigating intermediate-range atomic configurations around the Pd and Ni atoms reveals the existence of large-sized rings. Although the relation of the partial local structures and the glass-forming ability still remain unsolved, this paper will give a new insight in the structure-property relationship in metallic glasses. Noted that to our knowledge, the present work is the first experimental one that shows the existence of such large rings in a metallic glass with an excellent glass-forming ability.

ACKNOWLEDGMENTS

The authors acknowledge Prof. T. Usuki and Ms. A. Höhle, and Dr. D. Szubrin for the support of AXS and ND experiments, respectively. This work was performed under the inter-university cooperative research program of the Advanced Research Center of Metallic Glasses, Institute for Materials Research, Tohoku University (Project No. 11G0005 and 12G0022). The AXS experiments were performed at the beamline BM02 in the ESRF (Proposal No. ME1002, HD162, and HD426), and the neutron scattering measurements were carried out at ILL using the diffractometer D4 (Proposal No. 6–05–778). This work was supported by JSPS Grant-in-Aid for Scientific Research (C) (No. 22540403). AZ is supported by a Royal Society–EPSRC Dorothy Hodgkin Fellowship.

* Corresponding Author: shhosokawa@kumamoto-u.ac.jp

[1] H. S. Chen, Mater. Sci. Eng. **23**, 151 (1976).
[2] A. J. Drehman, A. L. Greer, and D. Turnbull, Appl. Phys. Lett. **41**, 716 (1982).
[3] H. W. Kui, A. L. Greer, and D. Turnbull, Appl. Phys. Lett. **45**, 615 (1984).
[4] H. W. Kui and D. Turnbull, Appl. Phys. Lett. **47**, 796 (1985).
[5] C. Park, M. Saito, Y. Waseda, N. Nishiyama, and A. Inoue, Mater. Trans. JIM **40**, 491 (1999).
[6] P. H. Gaskell, Nature (London) **276**, 484 (1978).
[7] O. Haruyama, K. Sugiyama, M. Sakurai, and Y. Waseda, J. Non-Cryst. Solids **353**, 3053 (2007).
[8] Y. Waseda, S. Kang, K. Sugiyama, M. Kimura, and M. Saito, J. Phys.: Condens. Matter **12**, A195 (2000).
[9] T. Egami, W. Dmowski, Y. He, and R. B. Schwarz, Metall. Mater. Trans. A **29A**, 1805 (1998).
[10] S. Hosokawa, J.-F. Bérar, N. Boudet, T. Ichitsubo, E. Matsubara, and N. Nishiyama, Mater. Trans. **48**, 2358 (2007).
[11] S. Hosokawa, J.-F. Bérar, N. Boudet, T. Ichitsubo, E. Matsubara, W.-C. Pilgrim, and N. Nishiyama, J. Phys.: Conf. Ser. **98**, 012013 (2008).
[12] S. Hosokawa, J.-F. Bérar, N. Boudet, T. Ichitsubo, E. Matsubara, and N. Nishiyama, J. Phys.: Conf. Ser. **144**, 012055 (2009).
[13] S. Hosokawa, H. Sato, T. Ichitsubo, M. Nakatake, N. Happo, J.-F. Bérar, N. Boudet, T. Usuki, W.-C. Pilgrim, E. Matsubara, and N. Nishiyama, Phys. Rev. B **80**, 174204 (2009).
[14] N. Nishiyama and A. Inoue, Appl. Phys. Lett. **80**, 568 (2002).
[15] S. Hosokawa, H. Sato, K. Mimura, N. Happo, Y. Tezuka, T. Ichitsubo, E. Matsubara, and N. Nishiyama, J. Electron Spectrosc. Relat. Phenom. **156-158**, 426 (2007).
[16] S. Hosokawa, H. Sato, N. Happo, K. Mimura, Y. Tezuka, T. Ichitsubo, E. Matsubara, and N. Nishiyama, Acta Mater. **55**, 3413 (2007).
[17] S. Hosokawa, H. Sato, N. Happo, T. Ichitsubo, E. Matsubara, and N. Nishiyama, Rev. Adv. Mater. Sci. **18**, 180 (2008).
[18] O. Haruyama, N. Annoshita, H. Kimura, N. Nishiyama, and A. Inoue, J. Non-Cryst. Solids **312314**, 552 (2002).
[19] S. R. Nagel and J. Tauc, Phys. Rev. Lett. **35**, 380 (1975).
[20] V. Kumar, T. Fujita, K. Konno, M. Matsuura, M. W. Chen, A. Inoue, and Y. Kawazoe, Phys. Rev. B **84**, 134204 (2011).
[21] P. F. Guan, T. Fujita, A. Hirata, Y. H. Liu, and M. W. Chen, Phys. Rev. Lett. **108**, 175501 (2012).
[22] J. L. Finney, Nature (London) **266**, 309 (1977).
[23] F. C. Franck, Proc. R. Soc. London, Ser. A **215**, 43 (1952).
[24] Y. Waseda, *Anomalous X-Ray Scattering for Materials Characterization* (Springer-Verlag, Deidelberg, 2002).
[25] R. L. McGreevy and L. Pusztai, Mol. Simul. **1**, 359 (1988).
[26] S. Hosokawa, W.-C. Pilgrim, J.-F. Bérar, and S. Kohara, Eur. Phys. J. Special Topics **208**, 291 (2012).
[27] H. E. Fischer, G. J. Cuello, P. Palleau, D. Feltin, A. C. Barnes, Y. S. Badyal, and J. M. Simonson, Appl. Phys. A **74**, S160 (2002).
[28] H. E. Fischer, A. C. Barnes, and P. S. Salmon, Rep. Prog. Phys. **69**, 233 (2006).
[29] S. Sasaki, *KEK Report 1989*, (Nat. Lab. High Energy Phys., Tsukuba, 1989), p. 1.
[30] C. H. MacGillavry and G. D. Rieck (ed.): *International Tables for X-ray Crystallographie*, 2nd ed., (Kynoch, Birmingham, 1968) Vol. III.
[31] S. Hosokawa, I. Oh, M. Sakurai, W.-C. Pilgrim, N. Boudet, J.-F. Bérar, and S. Kohara, Phys. Rev. B **84**, 014201 (2011).
[32] N. Metropolis, A. W. Rosenbluth, M. N. Rosenbluth, A. H. Teller, and E. Teller, J. Phys. Chem. **21**, 1087 (1953).
[33] O. Gereben, P. Jóvári, L. Temleitner, and L. Pusztai, J. Optoelectron. Adv. Mater. **9**, 3021 (2007).
[34] G. Voronoi, J. Reine Angew. Math., **133**, 97 (1908).
[35] Y. Hiraoka, T. Nakamura, A. Hirata, E. G. Escolar, K. Matsue, and Y. Nishiura, Proc. Natl. Acad. Sci. USA **113**, 7035 (2016).
[36] C. P. Chou and D. Turnbull, J. Non-Cryst. Solids **17**, 169 (1975).
[37] A. R. Yavari, K. Osamura, H. Okuda, and Y. Amemia, Phys. Rev. B **37**, 7759 (1988).
[38] J. D. Bernal, Nature **185**, 68 (1960).
[39] R. P. Messmer, Phys. Rev. B **23**, 1616 (1981).
[40] T. Fujiwara, J. Phys. F: Met. Phys. **12**, 661 (1982).
[41] H. S. Chen, Acta Metall. **22**, 1505 (1974).
[42] A. Inoue, T. Zhang, and T. Masumoto, J. Non-Cryst. Solids **156-158**, 473 (1993).
[43] H. Shintani and H. Tanaka, Nature Phys. **2**, 200 (2006).
[44] H. W. Sheng, W. K. Luo, F. M. Alamgir, J. M. Bai and E. Ma, Nature **439**, 419 (2006).
[45] N. Mattern, P. Jóvári, I. Kaban, S. Gruner, A. Elsner, V. Kokotin, H. Franz, B. Beuneu, and J. Eckert, J. Alloys Compd. **485**, 163 (2009).
[46] S. Hosokawa, J.-F. Bérar, N. Boudet, S. Kohara, W.-C. Pilgrim, M. Joester, J. Stellhorn, A. Zeidler, K. Maruyama, T. Nasu, W. Zhang, and H. Kato, Int. J. Mat. Res. **103**, 1108 (2012).
[47] M. Matsuura, W. Zhang, S. Yamaura, T. Fujita, K. Ohara, S. Kohara, and J. Mizuno, Mater. Trans. **54**, 1351 (2013).
[48] Y. He, T. Shen, and R. B. Schwarz, Metall. Mater. Trans. A **29**, 1795 (1998).